Computational Materials Science 214 (2022) 111693

Contents lists available at ScienceDirect

Computational Materials Science

journal homepage: www.elsevier.com/locate/commatsci

Full Length Article

An accurate computational model to study the Ag-doping effect on $SrTiO_3$

Sérgio A. Azevedo [a,b], José A.S. Laranjeira [a], Jesus L.P. Ururi [a,c], Elson Longo [c], Julio R. Sambrano [a,*]

[a] Modeling and Molecular Simulation Group, São Paulo State University – UNESP, 17033-360, Bauru, SP, Brazil
[b] Federal Institute of Maranhão – IFMA, 65950-000, Barra do Corda, Ma, Brazil
[c] CDMF, Federal University of São Carlos – UFSCar, 14801-907, São Carlos, SP, Brazil

ARTICLE INFO

Keywords:
$SrTiO_3$
Ag
DFT
Perovskite
Doping

ABSTRACT

Computational simulations via Density Functional Theory were carried out to study the effect of Ag-doping on $SrTiO_3$ and its properties. For accurate results, the coefficients of the Ag basis set were optimized, and the Hartree-Fock exchange parameter of the PBE0 functional was modified. It was found that the doping reduces the E_{gap} by 0.15 eV, modifying the indirect band gap to direct and transforming it from an *n*-type to a *p*-type semiconductor. The Crystal Orbital Hamilton Population (COHP) analysis revealed that the Ag-O bond was stronger for the anti-ligand states. The vibrational results showed that doping with Ag promoted a short-range structural disorder in the STO with the appearance of active Raman modes (Ag, B_{1g}, B_{2g}, and B_{3g}). Therefore, Ag is an appropriate metal for the doping of $SrTiO_3$ since it improves its optical absorption properties, thus opening up new possibilities for technology.

1. Introduction

The development of new materials with a wide range of applications occurs in several stages. The main one is through the creation of theoretical models close to real systems based on computational simulations linked to high-performance modeling software packages and the advancement of computational technology, which allow one to understand, among others, the structural, electronic, optical, vibrational, magnetic, thermoelectric and mechanical properties of such materials [1-12]. F90.

This work highlights a member of the perovskite family that is considered a functional material, $SrTiO_3$ (STO) [13-16] – an *n*-type semiconductor, which has an indirect band gap energy (E_{gap}) (~3.2 eV) and a cubic structure (*Pm-3 m*, a = 3.9 Å) [17-19]. Its properties can be improved or modified by the introduction of dopants [20-23]. In this context, Ghasemifard and coworkers [24] synthesized Ag- and Ba-doped STO by the combustion method and found a transition phase from cubic to tetragonal symmetry with a reduction of 0.06 eV in the band gap energy.

Among a wide variety of dopants, silver stands out for its well-known ability to improve the antimicrobial properties of materials when used in the form of ions [25-27], nanoparticles [28], and microstructures [29]. Nowadays, silver is regarded as a potent agent to fight SARS-Cov-2 [26,27]. For example, Tremiliosi et al. [30] developed an Ag-based polycotton fiber by the dry-pad-cure method and observed that the Ag nanoparticles promoted antimicrobial activity against *S. aureus*, *E. Coli*, *C. Albicans*, and SARS-CoV-2. Liu et al. [31] used Ag^+ ions to show the antibacterial activity and photoluminescent properties of Pr^{3+}-doped $CaTiO_3$. On the other hand, silver has also been used in plasmonic nanostructures with wide band gap semiconductors to remove the extension of light absorption to the visible range and improve their photocatalytic activity [12,24,32,33]. It must be mentioned that the use of silver to fight diseases has been a big challenge for experimental research groups and experts aiming to confirm or discard its efficiency. Indeed, this is also part of the challenges and achievements of modeling and computational research.

Concerning the theoretical research on STO, Van Benthem and coworkers [34], who carried out simulations based on the Density Functional Theory (DFT) in conjunction with the local density approximation (LDA) and an experimental study. The authors reported a conflicting result between the theoretical and experimental data, i.e., an indirect E_{gap} of 1.89 eV and a direct E_{gap} of 3.25 eV, respectively. Although a discrepancy between these observations was already expected since the LDA functional tends to overestimate the band gap value, there was a disagreement over the nature of the direct or indirect transition.

On the other hand, García-López et al. [35] synthesized the STO by

* Corresponding author.
E-mail address: sambrano@fc.unesp.br (J.R. Sambrano).

https://doi.org/10.1016/j.commatsci.2022.111693
Received 19 April 2022; Received in revised form 25 July 2022; Accepted 26 July 2022
Available online 4 August 2022

the Pechini synthesis method and obtained an indirect E_{gap} of 3.2 eV, corroborating the theoretical local density approximation (LDA) results on indirect E_{gap} reported by Benthen [34].

It is noteworthy that the indirect character of the gap involves the transition via phonons, which causes part of the incident energy to be wasted in these transitions, consequently impairing the efficiency of this material in optical applications [36]. To improve the optical efficiency of semiconductors, substitutional doping is the preferred method both to reduce the E_{gap} and to change the transition nature from indirect to direct [10].

Other theoretical studies corroborate the indirect nature of the E_{gap} of STO. For instance, Gillani et al. [9] simulated the STO using the DFT implemented in the CASTEP software with generalized gradient approximation (GGA) and Perdew-Burke-Ernzerhof functional (PBE) and calculated an indirect E_{gap} (R – Γ) of 1.792 eV and lattice parameters of 3.94 Å. Chen et al. [37] studied the STO using the DFT in the SIESTA code with GGA and a Hubbard correction parameter of 5 eV, and obtained an indirect gap (R-Γ) of 3.06 eV.

Pernot et al. [38] performed a benchmarking and validation study using the CRYSTAL14 code. The authors analyzed the lattice parameters, bulk modulus, and E_{gap} of a set of 28 crystals with cubic symmetry, and compared 18 different density functionals (local, semi-local, and hybrid functionals). The results indicated that the hybrid functionals are much superior to semi-local functionals in solid E_{gap} calculations due to the inclusion of the Hartree-Fock (HF%) exchange in the generalized Kohn-Sham formalism. Among the hybrid functionals, the PBE0 renders an accurate E_{gap} calculation for cubic structures, with an error of 0.55%.

There are several types of experimental research on metal-doped STO [10,36,39,40]. Particularly concerning the Ag-doped STO, although there is some theoretical research on this structure available in the literature, only a few studies focus on its electronic properties. For example, Qiu et al. [41] used plane wave functions to calculate the E_{gap} of Ag-doped STO at the Ti site, resulting in an indirect E_{gap} of 1.253 eV. Zhu et al. [42] used the DFT/PBE implemented in the Vienna Ab Initio Simulation Package (VASP) and the B3LYP functional in the CRYSTAL06 code to simulate Ag-doped STO at two metallic sites. According to the authors, Ag-Sr doping is more energetically favorable and promotes a drastic reduction in the E_{gap} in both software packages used (VASP 2.04 eV to 1.87 eV CRYSTAL06 3.44 eV to 2.88 eV). This research does not describe the Ag-Ti doping E_{gap}.

Considering the materials studied, STO is a stable semiconductor with several properties that make it an excellent ceramic material for doping and Ag is a metal with a high potential application. Therefore, the doping of STO with Ag aiming at new functional materials becomes extremely viable. Consequently, it is necessary to understand the effects of Ag on STO to develop a theoretical basis to support future experimental research and offer crucial information for the discovery of new properties of this material. Herein, the DFT applied to the systematic methodology is used to investigate the structural, electronic, and vibrational properties of Ag-doped STO. The results are discussed based on the analyses of the Density of States (DOS), band structures, Crystal Orbital Hamilton Populations (COHP), and Raman and infrared (IR) active modes, and compared with available experimental and theoretical data from the literature.

2. Computational method and model system

The computational simulations were performed within the framework of periodic DFT implemented in the CRYSTAL17 code [43]. This software is based on an original expansion of the crystalline wave function into a localized Gaussian-type basis set to represent the crystalline orbitals as a linear combination of Bloch functions. This work was used the PBE0 functional [44-46] and described strontium (Sr), titanium (Ti) and oxygen (O) using the Sr_HAYWSC-311(d11f)G[43], Ti_8-6411 (d311f)[47] and O_8-411 [48] basis set, respectively, where [HAYWSC] refers to the Hay-Wadt non-relativistic pseudopotential [49]. All basis sets are available in the Crystal library (www.crystal.unito.it/basis-sets.php). The crystallographic data of the STO cubic structure (*Pm-3m*) was obtained from JCPDS card No. 35–0734. Computational details can be found in the Supplementary Material.

Once the functional and the atomic basis set are established, it is necessary to select the best basis set for the Ag atom. To this end, two types of basis set were tested to describe the Ag atom valence double-zeta polarization (DZVP) [50] and Ag_extended_ruiz_2003 [43].

The energetically favorable metallic site was determined for the substitutional doping with Ag. Therefore, a 2x2x2 supercell containing 40 atoms (8 Sr, 8 Ti, and 24O) and eight bulk units ($SrTiO_3$) was constructed (Fig. 1a). To determine the most stable metallic site for doping, the doping energy (E_d) [51,52] was calculated according to the following formula

$E_d = E_{doped} - E_{undoped} - u_{Ag} + u_x(x = Sr\ or\ Ti)$, where E_{doped}, $E_{undoped}$, u_{Ag} and u_x are the total energies of the doped, undoped bulk, and chemical potential of Ag and Sr (or Ti) atoms, respectively, obtained from the total energy of each most stable metallic structure of the element [42].

As already expected, the Sr-site is more energetically favorable for doping, with $E_d = 4.66$ eV, while doping at the Ti-site has an $E_d = 15.86$ eV, confirming literature data [42]. Thus, STO doping was performed with both bases of Ag replacing Sr in the central position of the supercell (see Fig. 1b), resulting in a $Sr_7AgTi_8O_{24}$ stoichiometry (Ag-STO) and a doping percentage of 12.5%, which is compatible with experimental data [53,54].

Table 1 shows the results obtained from both Ag basis sets compared to those found in the literature [55]. It is possible to observe a good agreement between the experimental lattice parameters for both Ag basis sets however, the E_{gap} is significantly overestimated, and the doping does not change the nature of the E_{gap}.

It should be noted that the basis sets are not always adapted to the target system for this reason, when different basis sets already used for other systems are selected, it may be necessary to perform a new optimization of contraction coefficients or exponents [55]. However, each selected basis set is pre-designed and adapted to other systems. Consequently, when put together to simulate a new system, this may require

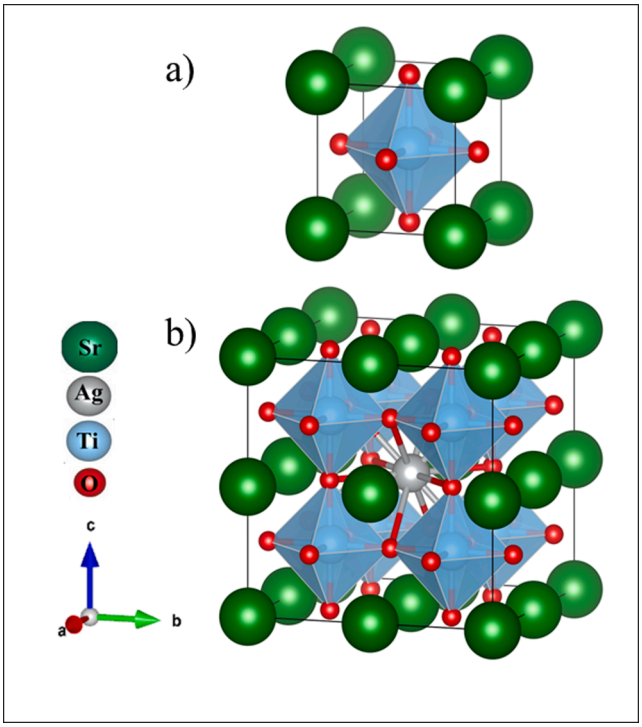

Fig. 1. a) STO bulk and b) Ag-STO 2x2x2 supercell.

Table 1
Lattice parameters (a, Å) and band gap energy (E_{gap}, eV) of Ag-STO.

Stoichiometry	a	E_{gap}	Nature
[1]Ag-STO*	3.89(-0.01)	4.15(+0.95)	Indirect (R – Γ)
[1]Ag-STO**	3.90	3.33(+0.13)	Indirect (R – Γ)
[1]Ag-STO***	3.88(-0.02)	3.19(-0.01)	Direct (Γ – Γ)
[2]Ag-STO	3.91	1.87	–
[2]Ag-STO	3.94	2.88	–
[3]Ag-STO	3.89	1.25	Indirect (R – Γ)
[4]STO	3.90	3.20	Indirect (R – Γ)

The brackets show the difference in relation to experimental data [17]. **Ag DZVP; Ag sll-electron (extended_ruiz_2003) [43], ***Ag optimized all-electron (extended_ruiz_2003) [47]. [1]This work (A = 16.5%); [2]DFT [42]. [3]DFT [41]. [4]Experimental [17].

an adaption to the target system.

Therefore, an optimization process of the selected Ag basis set must take place. Additionally, the computational cost, the steps for choosing the functional and the basis set, and the basis set optimization along with the Hartree Fock exchange percentage (HF) of the hybrid functional must also be considered.

At this point, an adequate procedure is to follow the algorithm proposed by Gomes et al. [55]. In this work, such a procedure was initially done by modifying the HF percentage and, when necessary, by performing a subsequent basis set optimization. Powell's [56] algorithm method was used for basis set optimization with the 10^{-6} Hartree energy convergence threshold [55]. The original basis set and the optimized coefficients are available in the Supplementary Material.

In the case of this study, the optimization process to minimize the total energy as a function of the exponents of the external basis set valence parameters α_p and α_d for the basis set Ag_extended_ruiz_2003 [43] aimed to obtain results of E_{gap} and lattice parameter closer to experimental ones (Tables 1 and 2).

The optimization of the Ag basis set led to an E_{gap} reduction of 0.14 eV compared to the original basis set (extended_ruiz_2003[43]) and 0.01 eV in relation to the reference band gap reported in the literature [17].

Table 3 shows the Ag-STO structure with the optimized Ag basis set, where it is possible to observe that the Ag-Ti (3.33 Å) bond length is smaller than the Sr-Ti (3.40 Å) bond, causing deformation in the [TiO_6] cluster and a reduction of 1.2°in the [$O - \widehat{Ti} - O$] bonding angle. Structural data demonstrate that doping with Ag slightly modifies the structural parameters of the STO, corroborating a similar result previously reported in theoretical studies on Ag-TiO_2 doping [57,58]. On the other hand, bond length and angles reflect a short-range disorder that creates new active vibrational modes, implying a change in the vibrational properties of the structure.

The band structure, DOS, and COHP were analyzed with the same k-point sampling employed for the diagonalization of the Fock matrix in the optimization process. The vibrational modes at the Γ-point were

Table 2
Optimized outer valence shell functions, α_p and α_d, of the selected basis set.

	Ag[a]	Ag[b]
α_p	2.505	1.907
	1.042	1.797
α_d	310.274	310.312
	91.144	91.271
	33.219	33.315
	12.983	13.108
	5.013	5.122
	3.391	5.207
	1.599	0.708
	0.628	0.671

[a] Ag basis set coefficients (extended_ruiz_2003)[43] and [b]coefficients after optimization.

Table 3
Bond length (Å) and bond angle (degree) of Ag-STO.

Length	Angle
Sr—Ag = 3.88	[O—Ag—O] = 60°
Ti—Ag = 3.33	[Ti—Ag—Ti] = 70.5°
Ag—O = 2.74	[O—Ti—O] = 178.8°
Ti—O = 1.96	
Sr—Ti = 3.40	
Sr—O = 2.76	

evaluated using the numerical second derivatives of the total energies estimated with the coupled perturbed HF/Kohn-Sham algorithm [59].

The parameters described below were used in all calculations performed in the present study. The precision of Coulomb and exchange infinite series was controlled by five thresholds, i.e., 10^{-8}, 10^{-8}, 10^{-8}, 10^{-8}, and 10^{-16}, which represent the overlap and penetration for Coulomb integrals, the overlap for HF exchange integrals, and the pseudo-overlap, respectively. Energy convergence parameters based on the self-consistent field theory for the geometrical optimization and frequency calculations were set to 10^{-10} Ha. In contrast, the shrinking factor (Pack-Monkhorst and Gilat nets) was set to 8 for the STO and Ag-STO[60]. The Raman modes were calculated using the coupled perturbed Hartree-Fock/Kohn-Sham method[61].

3. Results and discussion

3.1. Electronic properties

Fig. 2a and 2b illustrate the band structure of the STO and Ag-STO. The results show that the E_{gap} of the STO is indirect (3.34 eV) at R – Γ points, which is in agreement with what was predicted in the literature [17]. Substitutional doping with Ag decreased the E_{gap} by 0.15 eV. Furthermore, Ag changed the nature of the band gap from indirect to direct (Γ – Γ), increasing the Fermi energy (E_f) by 1.17 eV and resulting in the allocation of the valence band (VB) and the conduction band (CB) to more significant energy levels. This was attributed to the formation of [Ag—O] bonds, and consequently to the emergence of the new states near the region of the VB maximum and the CB minimum. On the other hand, metallic silver increased electron transfer from the semiconductor. These modifications in the STO may enhance the photocatalytic activity and the two-way photoconductivity of the material as a result of improved radiation absorption caused by the increased electronic recombination compared to the undoped STO – where phonon emission is a necessary step before the occurrence of radiative recombination in the system[36]. These results had already been confirmed in an experimental study carried out by Shi et al.[62], who synthesized STO with the (1 1 1) surface deposition of Ag nanoparticles. The authors observed a better dynamic in electron transfer and a reduction in the radiative recombination rate, indicating the occurrence of a direct band gap due to the improved optical properties of the STO. The band structure of Ag-STO suggests that doping with Ag may develop photoluminescent properties in the STO. This corroborates the work by Longo et al. [63], who conducted a theoretical and experimental study on STO and verified that structural changes in the lattice modifier (Sr) can create a short-range disorder in the [TiO_6] cluster, with a consequent reduction in the E_{gap} caused by new states above E_f, resulting in photoluminescent properties in the STO semiconductor.

The DOS of the STO (Fig. 2c) shows that the O and Ti atoms have the highest electronic contributions in the VB and CB, respectively, while the Sr atom has the lowest contribution in both bands. Furthermore, the region close to the VB maximum is formed primarily by [Ti—O] interactions, implying that the optical properties of STO are slightly associated with these interactions.

Regarding the Ag-STO, the DOS (Fig. 2d) demonstrates that the Ag-doping altered the electronic states in the band gap region, with the

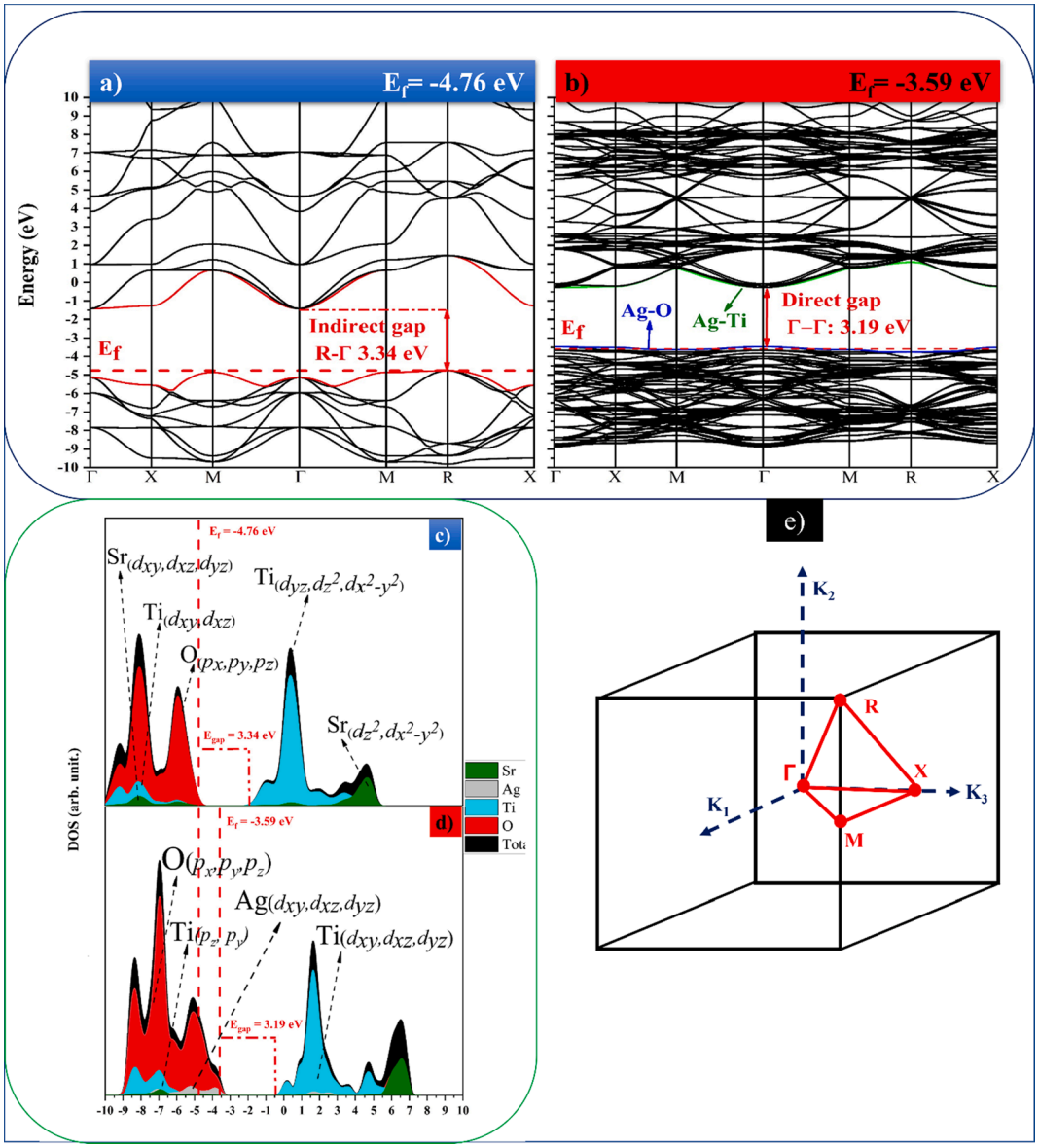

Fig. 2. a) and b) STO and Ag-STO band structures, respectively, c) and d) STO and Ag-STO DOS, respectively, and e) first Brillouin zone with high symmetry points.

oxygen atom retaining a higher DOS in the VB and the Ag atom influencing the reduction of Ti states in the VB with predominant bonding states [Ag—O] in the VB maximum region. In contrast, the electronic states in the CB are derived from Ti, O and Ag atoms, with a predominance of electron density arising from [Ti—O] bonds and a reduction of 0.15 eV in E_g – which occurs due to the introduction of new states from the linear combination of orbitals (*d, p,* and *s*) of [Ag—O] bonds at the VB maximum and [Ti—O] and [Ag—Ti] bonds at the CB minimum. It should be noted that the Sr atom does not exhibit states at the VB maximum and the CB minimum.

The partial density of states (PDOS) for the Ag-STO orbitals (Fig. 3) indicates that the electron density of O atoms comes from triply degenerate *p*-type orbitals. While the Sr atom has no *d*-type orbital density in the VB, converging with the configuration of the Sr^{2+} ion (which has a $4p^6 5s^0$ valence configuration), the Ti atom has a valence configuration in the Ti^{+4} ($4s^0 3d^0$) oxidation. However, as shown in Fig. 3, the DOS derives from $4p_z$ and $4p_y$ degenerate orbitals and the hybridization occurs in the *sp*-type CB ($5\,s + 4p_x$), which has unfolding in the crystalline field of *d* orbitals due to a breakdown of symmetry of d_{xy}, d_{xz} and d_{yz} (symmetry t_{2g}) as well as $d^2_{x^2-y^2}$ and d_{z^2} (symmetry e_g). The Ag atom in the CB region has a DOS arising from 4d orbitals, with a slight unfolding in the crystalline field between the $d^2_{x^2-y^2}$, $d^2_{z^2}$ (symmetry e_g) and d_{xy}, d_{xz}, d_{yz} (t_{2g} symmetry) orbitals. It should be highlighted that the orbitals with e_g symmetry has lower energy, and consequently higher electron contribution. Because the electronic interaction in the VB occurs in the [Ag—O] bond (with a predominance of *d* Ag and *p* O states), the substitution of Ag by Sr favors a short-range disorder in the [TiO_6] octahedron.

Overall, the doping significantly altered the electronic properties of the STO by inhibiting Sr states in the VB region and significantly changing the crystalline unfolding of Ti and Sr *d* orbitals in both the VB and the CB (Figure S2 in the Supplementary Material).

Fig. 4a and 4b reveal the charge maps of the STO and Ag-STO structures, with a cut section in the (1 1 0) plane exhibiting the chemical bonds of the atomic species inside the structure. The red region represents an accumulation of negative charges caused by polarization of the covalent bond, whereas the blue region corresponds to an area of low polarization of negative charges.

By analyzing the charge density map of the STO and Ag-STO structures, the interactions observed between Ti and O atoms are covalent bonds, while between Sr and O atoms, there are electrostatic interactions characterized by ionic bonding. Despite the higher

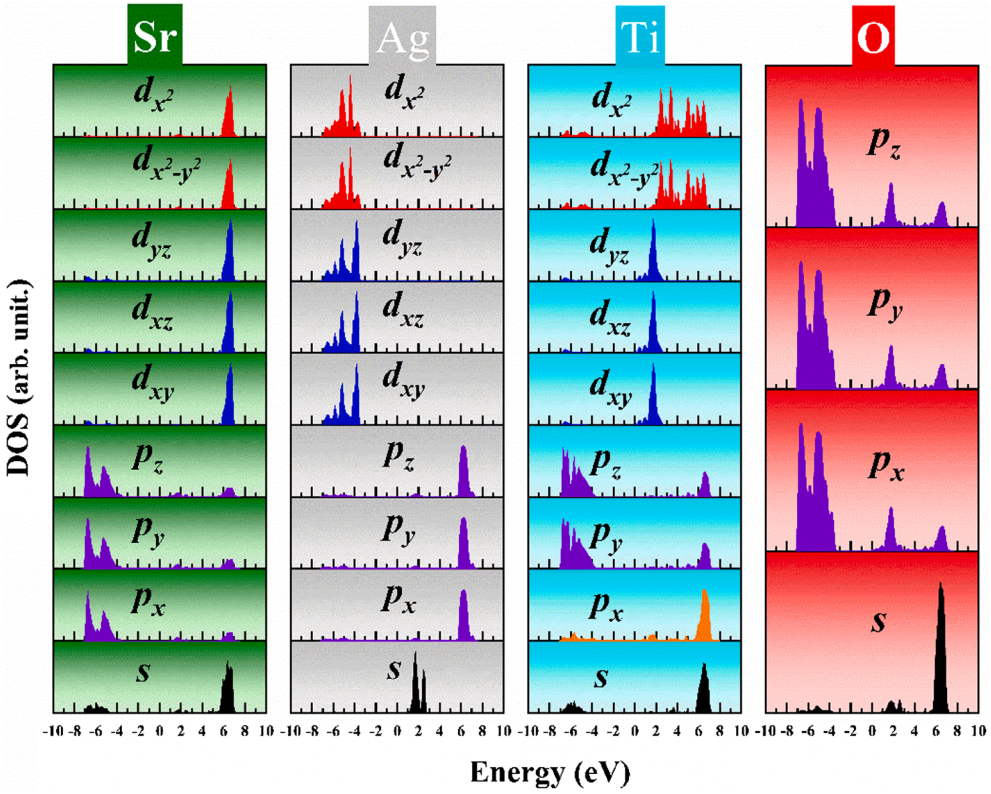

Fig. 3. Projected DOS for the orbitals of Ag-STO.

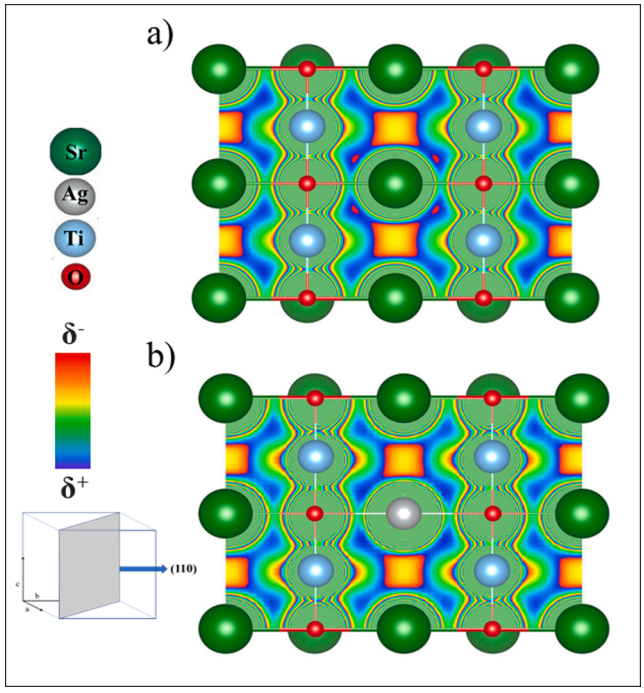

Fig. 4. Charge density map a) STO and b) Ag-STO.

electronegativity of Ag to Sr, the replacement of Sr by Ag in both structures demonstrates that the substitutional doping does not promote any changes in the nature of chemical bonds in the structure, as both structures are characterized by electron clouds referring to covalent and ionic bonds.

The analysis of atomic charges of the STO (Sr = +1.919, Ti = +2.456, O = -1.468) and Ag-STO (Ag = +0.836, Sr = +1.800, Ti = +2.232, O = -1.368 and −1.256) by the Hirshfeld's method [64,65] shows that Ag decreases the charge of Ti and Sr and increases the charge of O as a result of the electron-hole reorganization promoted by the appearance of a hole created by the oxidation difference during the replacement of Sr^{2+} by Ag^{1+} in the doping process, causing the Ag-STO to become an extrinsic *p*-type semiconductor.

COHP calculations were carried out to interpret the Ag interaction, in which the energy of the band structure is partitioned, yielding information about the bonding and antibonding nature of the chemical bond between two elements [66]. In the VB region of the COHP plot (Fig. 5a), there is a predominant Ag-O interaction with a combination of antibonding orbitals in the regions with energy of −4.0 eV. In addition, it can be seen that the bond is stronger at the top of the VB due to overlapping bonding orbitals. Because of the electron density of these elements in their respective valence layers, the region of negative overlap of Ag-Ti orbitals reveals a weak covalent bond between these two species. The ICOHP data were obtained by integrating the COHP curve, which indicated that the strongest Ag bond occurs in the Ag-O interaction due to a smaller number of antibonding molecular orbitals arising from the overlapping orbitals of the elements.

The Ag-O bond is formed by the interaction of *d* orbitals of Ag and *p* orbitals of O. The COHP data (Fig. 5b) of these interactions demonstrate the strongest bond of the combination of Ag orbitals (d_{xy}, d_{xz}, d_{yz}) and O orbitals (p_x, p_y, p_z) resulting from the out-of-plane interactions configuring a π-type chemical bond.

3.2. Vibrational properties

At room temperature, the cubic structure of STO has 3 acoustic and 12 optical modes [10]. At point Γ, there are 3 polar optical modes along with acoustic modes and a non-polar triply degenerate mode (with all active vibrational modes of the structure in the infrared (IR) region), where the 3 IR active degenerate F_{1u} modes correspond to the acoustic

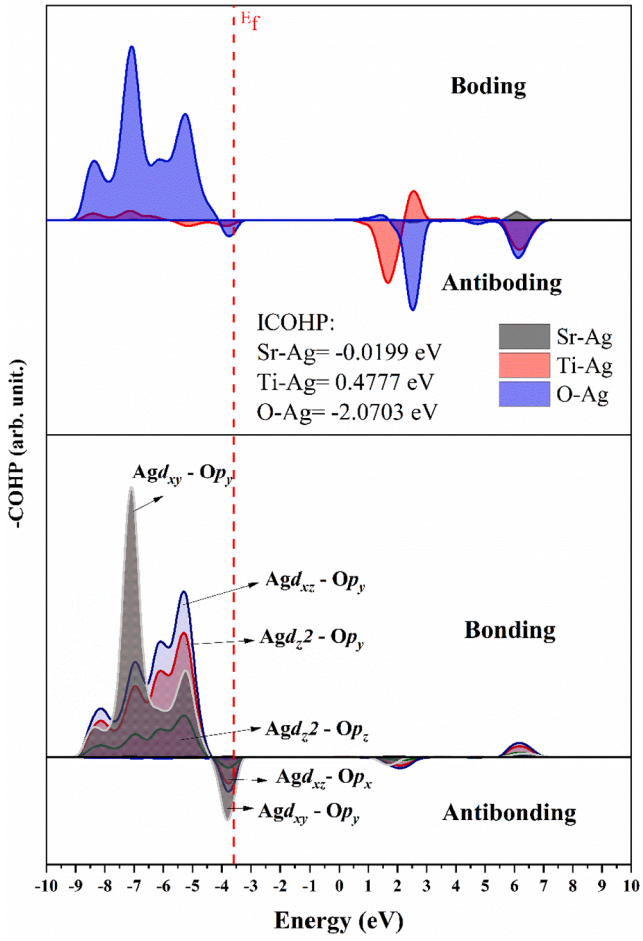

Fig. 5. COHP of the Ag-STO structure a) interaction between constituents and b) interaction of Ag–O orbitals.

mode, while the inactive F_{2u} modes correspond to an optically silent mode (see Figure S3 in the Supplementary Material).

Fig. 6 shows the infrared and Raman spectra of the Ag-STO structure. It can be observed that the structure has irreducible symmetric $\Gamma = A_g + B_{1g} + B_{3g} + B_{2g} + B_{1u} + B_{2u} + B_{3u}$ with 120 vibrational modes, among

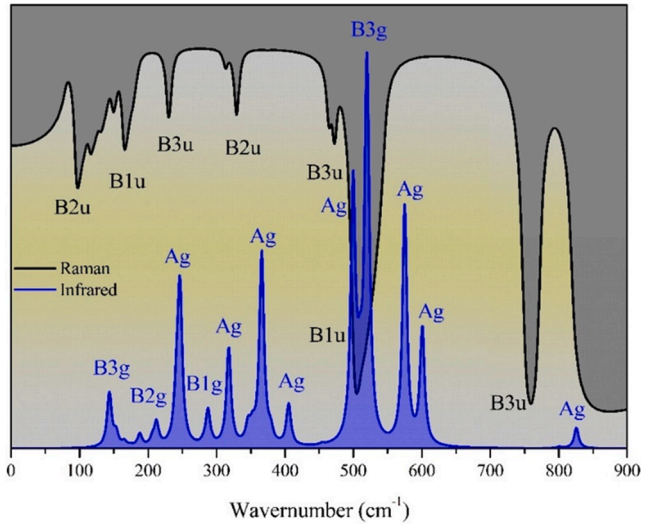

Fig. 6. IR and Raman spectra of Ag-STO. (For more details, see the video in the Supplementary Material).

which 62 are IR active modes ($20B_{1u} + 21B_{2u} + 21B_{3u}$), 48 are Raman active modes ($14A_g + 12B_{1g} + 11B_{3g} + 11B_{2g}$) and 10 are optically silent inactive A_u-type modes.

The B_{1u} symmetry in the region of 199 cm^{-1} in the active IR modes refers to symmetrical axial deformations in all structure atoms. On the other hand, at 503 cm^{-1}, that is, the region with higher vibrational absorption in the IR, there is a symmetrical angular deformation in the plane of O atoms in the [Ti—O] bond. The B_{2u} symmetry represents a bending angular deformation of O atoms in the [Ti—O] bond. At 80 cm^{-1} there is a symmetrical angular twist outside the plane of Sr atoms. Finally, the low-frequency B_{3u} modes are symmetrical and asymmetrical angular deformations in the plane. At 772 cm^{-1}, it is possible to observe an axial deformation due to symmetrical stretching (see Figure S4 in Supplementary Material).

In the IR active modes, the Ag symmetry refers to symmetrical and asymmetrical angular deformations in the plane of the [Ti—O] bond, except for the 825 cm^{-1} frequency mode, which corresponds to the symmetrical stretching mode of the [Ti—O] bond. B_{1g} is the out-of-plane symmetrical angular strain of the [Ti—O] bond. Regarding B_{2g}, at a frequency of 165 cm^{-1} it is an out-of-plane asymmetrical angular strain of Ti atoms of the [TiO_6] cluster, whereas, at 212 cm^{-1} there is a symmetrical angular deformation in the plane of O atoms in the [Ti—O] bond. Lastly, the B_{3g} symmetry is an asymmetrical, angular deformation outside the plane of Ti atoms at 143 cm^{-1} and O atoms at 521 cm^{-1} of the [TiO_6] cluster (see Figure S4 in the Supplementary Material).

In summary, the vibrational results show that at low frequencies, the metals present in the structure suffer more significant vibrational effects. In addition, the structure stability is strongly dependent on the [TiO_6] cluster, considering that the most crucial number of vibrational modes are vibrations of the [Ti—O] bonds. In contrast, at high frequencies the vibrational modes are stretching in both spectra (IR and Raman).

Therefore, the emergence of Raman active modes as a result of the replacement of Sr by Ag in the doping process promotes a short-range disorder in the interaction between titanium and oxygen atoms of the Ti-O cluster. The existence of Ag, B_{1g}, B_{1g}, and B_{3g} symmetry modes suggests that there may be a change in symmetry in the doped system from *Pm-3m* to *I4-mcm* – which in the STO structure only occurs at temperatures below 105 K[67].

4. Conclusion

The computational study using DFT simulations was fundamental to understanding the effects of Ag-doping on $SrTiO_3$. Based on the findings, it can be inferred that the optical absorption and emission properties of the Ag-STO structure are derived from Ag, since the interactions of states near the top and bottom of the valence and conduction bands are dominated by the [Ag—O] bond, resulting in a band gap change from indirect (R – Γ) to direct (Γ – Γ) and a reduction in the STO band gap value. The STO doping with Ag creates an electron hole, causing the Ag-$SrTiO_3$ to become a *p*-type semiconductor. The COHP data show that the Ag has a strong bonding with O and an almost non-existent bonding with Sr. Additionally, the [Ag - O] bond has a strong antibonding region in the innermost part of the VB and a strong bonding interaction at the VB maximum.

According to the analysis of vibrational properties of the material, there are 120 new active modes resulting from a short-range disorder in the chemical bonds.

For such reasons, Ag appears to be an appropriate metal for doping, as it does not cause changes in the STO symmetry and improves its electronic properties by switching the band gap from indirect to a direct gap, making this semiconductor more effective in optical applications. Therefore, the STO doping with Ag is a promising alternative for the development of new materials with multiple functionalities.

CRediT authorship contribution statement

Sérgio A. Azevedo: Conceptualization, Investigation, Methodology, Software, Validation, Formal analysis, Writing – original draft, Writing – review & editing. **José A.S. Laranjeira:** Data curation, Visualization, Formal analysis, Writing – original draft. **Jesus L.P. Ururi:** Writing – original draft. **Elson Longo:** Funding acquisition. **Julio R. Sambrano:** Conceptualization, Funding acquisition, Investigation, Methodology, Project administration, Resources, Software, Supervision, Validation, Visualization, Writing – original draft, Writing – review & editing.

Declaration of Competing Interest

The authors declare that they have no known competing financial interests or personal relationships that could have appeared to influence the work reported in this paper.

Data availability

Data will be made available on request.

Acknowledgments

This work was supported by the following Brazilian funding agencies FAPESP (2019/08928-9, 2013/07296-2, 2020/10380-9, 2020/01144-0 and 2022/03959-6) and CNPq (307213/2021-8). The computational facilities were supported by resources supplied by the Laboratory of Molecular Simulations, São Paulo State University – UNESP, Bauru, Brazil. Besides, we would like to thank the Federal Institute of Maranhão – IFMA, which granted a license and financially supported Azevedo S. A.

Appendix A. Supplementary material

Supplementary data to this article can be found online at https://doi.org/10.1016/j.commatsci.2022.111693.

References

[1] Z. Zhao, E. Li, Y. Qin, X. Liu, Y. Zou, H. Wu, T. Zhu, Density functional theory (DFT) studies of vanadium-titanium based selective catalytic reduction (SCR) catalysts, J. Environ. Sci. (China). 90 (2020) 119–137, https://doi.org/10.1016/j.jes.2019.11.008.
[2] P. Scharoch, M. Winiarski, An efficient method of DFT/LDA band-gap correction, Comput. Phys. Commun. 184 (2013) 2680–2683, https://doi.org/10.1016/j.cpc.2013.07.008.
[3] M. Ribeiro, Electronic band gaps corrections using total energy with DFT/LDA-½ quasi-particle approximation, Comput. Mater. Sci. 167 (2019) 228–236, https://doi.org/10.1016/j.commatsci.2019.05.048.
[4] A.D. Laurent, D. Jacquemin, TD-DFT benchmarks a review, Int. J. Quantum Chem. 113 (2013) 2019–2039, https://doi.org/10.1002/qua.24438.
[5] K. Ryczko, D.A. Strubbe, I. Tamblyn, Deep learning and density-functional theory, Phys. Rev. A 100 (2019), https://doi.org/10.1103/PhysRevA.100.022512.
[6] J. Landers, G.Y. Gor, A.V. Neimark, Density functional theory methods for characterization of porous materials, Colloids Surf. A Physicochem. Eng. Aspects. 437 (2013) 3–32, https://doi.org/10.1016/j.colsurfa.2013.01.007.
[7] J. Neugebauer, T. Hickel, Density functional theory in materials science, wiley interdisciplinary reviews computational molecular, Science 3 (2013) 438–448, https://doi.org/10.1002/wcms.1125.
[8] A.H. Reshak, Thermoelectric properties of Srn+1TinO3n+1 (n=1, 2, 3, ∞) ruddlesden-popper homologous series, Renew. Energy 76 (2015) 36–44, https://doi.org/10.1016/j.renene.2014.11.006.
[9] S.S.A. Gillani, R. Ahmad, Islah-u-din, M. Rizwan, M. Shakil, M. Rafique, G. Murtaza, H.B. Jin, First-principles investigation of structural, electronic, optical and thermal properties of Zinc doped SrTiO3, Optik (Stuttg). 201 (2020). 10.1016/j.ijleo.2019.163481.
[10] M.N. Gastiasoro, J. Ruhman, R.M. Fernandes, Superconductivity in dilute SrTiO3 a review, Ann. Phys. 417 (2020), https://doi.org/10.1016/j.aop.2020.168107.
[11] R.B. Ahirrao, S.R. Khatik, Materials Today Proceedings Photoconductivity study of spray pyrolized pure and Cu-modified SrTiO3 thin films, Mater. Today Proceedings. (2020), https://doi.org/10.1016/j.matpr.2020.05.517.
[12] Z. Liu, Z. Ma, Ag-SrTiO3/TiO2 composite nanostructures with enhanced photocatalytic activity, Mater. Res. Bulletin J. 118 (2019), https://doi.org/10.1016/j.materresbull.2019.110492.
[13] D.D. Athayde, D.F. Souza, A.M.A. Silva, D. Vasconcelos, E.H.M. Nunes, J.C.D. Da Costa, W.L. Vasconcelos, Review of perovskite ceramic synthesis and membrane preparation methods, Ceram. Int. 42 (2016) 6555–6571, https://doi.org/10.1016/j.ceramint.2016.01.130.
[14] G.R. Adams, O.I. Okoli, A review of perovskite solar cells with a focus on wire-shaped devices, Renew. Energy Focus. 25 (2018) 17–23, https://doi.org/10.1016/j.ref.2018.02.002.
[15] Y. Yin, Q. Li, A review on all-perovskite multiferroic tunnel junctions, J. Materiomics 3 (2017) 245–254, https://doi.org/10.1016/j.jmat.2017.09.001.
[16] E. Rahmatizad Khajehpasha, S. Goedecker, S.A. Ghasemi, New strontium titanate polymorphs under high pressure, J. Comput. Chem. 42 (2021) 699–705, https://doi.org/10.1002/jcc.26490.
[17] G. Wang, Y. Qin, J. Cheng, Y. Wang, Influence of Zn doping on the photocatalytic property of SrTiO3, J. Fuel Chem. Technol. 38 (2010) 502–507, https://doi.org/10.1016/S1872-5813(10)60042-4.
[18] Y. Du, M.S. Zhang, J. Wu, L. Kang, S. Yang, P. Wu, Z. Yin, Optical properties of SrTiO3 thin films by pulsed laser deposition, Appl. Phys. A Mater. Sci. Processing. 76 (2003) 1105–1108, https://doi.org/10.1007/s00339-002-1998-z.
[19] X.L. Shi, H. Wu, Q. Liu, W. Zhou, S. Lu, Z. Shao, M. Dargusch, Z.G. Chen, SrTiO3-based thermoelectrics progress and challenges, Nano Energy 78 (2020), https://doi.org/10.1016/j.nanoen.2020.105195.
[20] B. King, Minerals explained 57 Perovskite, Geol. Today 20 (2004) 34–37, https://doi.org/10.1111/j.1365-2451.2004.00444.x.
[21] D. Fu, M. Itoh, Ferroelectricity in Silver Perovskite Oxides, in Ferroelectrics, Material Aspects, 2011. 10.5772/17261.
[22] G.A.S. Alves, H.A. Centurion, J.R. Sambrano, M.M. Ferrer, R. v. Gonçalves, Band Gap Narrowing of Bi-Doped NaTaO3 for Photocatalytic Hydrogen Evolution under Simulated Sunlight A Pseudocubic Phase Induced by Doping, ACS Applied Energy Materials. 4 (2021) 671–679. 10.1021/ACSAEM.0C02547/SUPPL_FILE/AE0C02547_SI_001.PDF.
[23] C. Shi, M. Morinaga, Doping effects on proton incorporation and conduction in SrZrO3, J. Comput. Chem. 27 (2006) 711–718, https://doi.org/10.1002/jcc.20381.
[24] M. Ghasemifard, M.E. Abrishami, M. Iziy, Effect of different dopants Ba and Ag on the properties of SrTiO3 nanopowders, Results Phys. 5 (2015) 309–313, https://doi.org/10.1016/j.rinp.2015.10.005.
[25] R. Vazquez-Munoz, J.L. Lopez-Ribot, Nanotechnology as an Alternative to Reduce the Spread of COVID-19, Challenges. 11 (2020) 15, https://doi.org/10.3390/challe11020015.
[26] S.S. Jeremiah, K. Miyakawa, T. Morita, Y. Yamaoka, A. Ryo, Potent antiviral effect of silver nanoparticles on SARS-CoV-2, Biochem. Biophys. Res. Commun. 533 (2020) 195–200, https://doi.org/10.1016/j.bbrc.2020.09.018.
[27] C. Balagna, S. Perero, E. Percivalle, E.V. Nepita, M. Ferraris, Virucidal effect against coronavirus SARS-CoV-2 of a silver nanocluster/silica composite sputtered coating, Open Ceramics. 1 (2020), 100006, https://doi.org/10.1016/j.oceram.2020.100006.
[28] S.P. Deshmukh, S.M. Patil, S.B. Mullani, S.D. Delekar, Silver nanoparticles as an effective disinfectant a review, Mater. Sci. Eng., C 97 (2019) 954–965, https://doi.org/10.1016/j.msec.2018.12.102.
[29] M.D. Penha, A.F. Gouveia, M.M. Teixeira, R.C. de Oliveira, M. Assis, J. R. Sambrano, F. Yokaichya, C.C. Santos, R.F. Gonçalves, M. Siu Li, M.A. San-Miguel, J. Andrés, E. Longo, Structure, optical properties, and photocatalytic activity of α-Ag2W0.75Mo0.25O4, Mater. Res. Bull. 132 (2020), 111011, https://doi.org/10.1016/j.materresbull.2020.111011.
[30] G.C. Tremiliosi, L.G.P. Simoes, D.T. Mi-, R.I. Santos, D.C.B. Vilela, E.L. Durigon, R. R.G. Machado, D.F. Sales-medina, C. Alexandre, L.K. Ribeiro, I.L. V Rosa, M. Assis, J. An-, E. Longo, L.H. Freitas-junior, Engineering polycotton fiber surfaces, with an timicrobial activity against S. aureus, E. Coli, C. albicans and SARS-CoV-2, Japan Journal of Medical Science. 1 (2020) 47–58.
[31] Z. Liu, K. Qiu, Q. Tang, Y. Wu, J. Wang, Synthesis of Ag+/CaTiO3:Pr3+ with luminescence and antibacterial properties, Adv. Powder Technol. 30 (2019) 23–29, https://doi.org/10.1016/j.apt.2018.10.003.
[32] Q. Zhang, Y. Huang, L. Xu, J.J. Cao, W. Ho, S.C. Lee, Visible-Light-Active Plasmonic Ag-SrTiO3 Nanocomposites for the Degradation of NO in Air with High Selectivity, ACS Appl. Mater. Interfaces 8 (2016) 4165–4174, https://doi.org/10.1021/acsami.5b11887.
[33] S. Patial, V. Hasija, P. Raizada, P. Singh, A.A.P. Khan Singh, A.M. Asiri, Tunable photocatalytic activity of SrTiO3 for water splitting strategies and future scenario, J. Environ. Chem. Eng. 8 (2020), https://doi.org/10.1016/j.jece.2020.103791.
[34] K. Van Benthem, C. Elsässer, R.H. French, Bulk electronic structure of SrTiO3 experiment and theory, J. Appl. Phys. 90 (2001) 6156–6164, https://doi.org/10.1063/1.1415766.
[35] E. García-López, G. Marcì, B. Megna, F. Parisi, L. Armelao, a. Trovarelli, M. Boaro, L. Palmisano, SrTiO3-based perovskites Preparation, characterization and photocatalytic activity in gas–solid regime under simulated solar irradiation, Journal of Catalysis. 321 (2015) 13–22. 10.1016/j.jcat.2014.10.014.
[36] M. Rizwan, A. Ali, Z. Usman, N.R. Khalid, H.B. Jin, C.B. Cao, Physica B condensed Matter Structural, electronic and optical properties of copper-doped SrTiO 3 perovskite a DFT study, Phys. B Condensed Matter. 552 (2019) 52–57, https://doi.org/10.1016/j.physb.2018.09.022.
[37] A. Chen, S.V. Nair, B. Miljkovic, C. Souza, H.E. Ruda, Z. Ji, Electronic structure of bulk and two-dimensional SrTiO3 DFT calculation with GGA + U methods, J. Nanopart. Res. 22 (2020), https://doi.org/10.1007/s11051-020-04994-5.
[38] P. Pernot, B. Civalleri, D. Presti, A. Savin, Prediction uncertainty of density functional approximations for properties of crystals with cubic symmetry, J. Phys. Chem. A 119 (2015) 5288–5304, https://doi.org/10.1021/jp509980w.

[39] H.A. Maddah, V. Berry, S.K. Behura, Biomolecular photosensitizers for dye-sensitized solar cells recent developments and critical insights, Renew. Sustain. Energy Rev. 121 (2020), 109678, https://doi.org/10.1016/j.rser.2019.109678.
[40] B. Zhong, Z. Long, C. Yang, Y. Li, X. Wei, Colossal dielectric permittivity in co-doping SrTiO3 ceramics by Nb and Mg, Ceram. Int. 46 (2020) 20565–20569, https://doi.org/10.1016/j.ceramint.2020.05.174.
[41] B. Qiu, X.G. Yan, W.Q. Huang, G.F. Huang, C. Jiao, S.Q. Zhan, J.P. Long, Z. M. Yang, Z. Wan, P. Peng, The electronic and optical properties of X-doped SrTiO3 (X = Rh, Pd, Ag) a first-principles calculations, Int. J. Mod Phys B 28 (2014) 1–11, https://doi.org/10.1142/S0217979214500313.
[42] Y. Zhu, Y. Dai, W. Wei, B. Huag, First principles study of Ag-doped, Nb-doped and Ag/Nb doped SrTiO3, Rare Met. 30 (2011) 177–182, https://doi.org/10.1007/s12598-011-0264-y.
[43] R. Dovesi, A. Erba, R. Orlando, C.M. Zicovich-Wilson, B. Civalleri, L. Maschio, M. Rérat, S. Casassa, J. Baima, S. Salustro, B. Kirtman, Quantum-mechanical condensed matter simulations with CRYSTAL, wiley interdisciplinary reviews computational molecular, Science 8 (2018) 1–36, https://doi.org/10.1002/wcms.1360.
[44] J.P. Perdew, K. Burke, M. Ernzerhof, Generalized gradient approximation made simple, Phys. Rev. Lett. 77 (1996) 3865–3868, https://doi.org/10.1103/PhysRevLett.77.3865.
[45] C. Adamo, V. Barone, Toward reliable density functional methods without adjustable parameters the PBE0 model, J. Chem. Phys. 110 (1999) 6158–6170, https://doi.org/10.1063/1.478522.
[46] M. Ernzerhof, G.E. Scuseria, Assessment of the Perdew – Burke –, Ernzerhof 110 (1999) 5029–5036.
[47] A. Erba, K.E. El-Kelany, M. Ferrero, I. Baraille, M. Rérat, Piezoelectricity of SrTiO3 an ab initio description, Phys. Rev. B - Condensed Matter and Mater. Phys. 88 (2013) 1–10, https://doi.org/10.1103/PhysRevB.88.035102.
[48] J. Scaranto, S. Giorgianni, A systematic study of the influence of the slab thickness on the Lewis acidity of the rutile (1 1 0) surface a quantum-mechanical simulation of CO adsorption, Chem. Phys. Lett. 473 (2009) 179–183, https://doi.org/10.1016/j.cplett.2009.03.036.
[49] M.P. Habas, R. Dovesi, A. Lichanot, The B1 ⇌ B2 phase transition in alkaline-earth oxides a comparison of ab initio Hartree-Fock and density functional calculations, J. Phys.: Condens. Matter 10 (1998) 6897–6909, https://doi.org/10.1088/0953-8984/10/31/008.
[50] J. Laun, D. Vilela Oliveira, T. Bredow, Consistent gaussian basis sets of double- and triple-zeta valence with polarization quality of the fifth period for solid-state calculations, J. Comput. Chem. 39 (2018) 1285–1290, https://doi.org/10.1002/jcc.25195.
[51] N. Li, K.L. Yao, The electronic and optical properties of carbon-doped SrTiO3 density functional characterization, AIP Adv. 2 (2012), https://doi.org/10.1063/1.4746023.
[52] A.R. Albuquerque, A. Bruix, I.M.G. dos Santos, J.R. Sambrano, F. Illas, DFT study on Ce-doped anatase TiO2 nature of Ce3+ and Ti3+ centers triggered by oxygen vacancy formation, J. Phys. Chem. C 118 (2014) 9677–9689, https://doi.org/10.1021/jp501757f.
[53] D. Park, H. Ju, J. Kim, One-pot fabrication of Ag–SrTiO3 nanocomposite and its enhanced thermoelectric properties, Ceram. Int. 45 (2019) 16969–16975, https://doi.org/10.1016/j.ceramint.2019.05.245.
[54] S. Wan, M. Chen, M. Ou, Q. Zhong, Plasmonic Ag nanoparticles decorated SrTiO3 nanocubes for enhanced photocatalytic CO2 reduction and H2 evolution under visible light irradiation, J. CO2 Util. 33 (2019) 357–364, https://doi.org/10.1016/j.jcou.2019.06.024.
[55] E.O. Gomes, G.S.L. Fabris, M.M. Ferrer, F. v. Motta, M.R.D. Bomio, J. Andres, E. Longo, J.R. Sambrano, Computational procedure to an accurate DFT simulation to solid state systems, Computational Materials Science. 170 (2019) 109176. 10.1016/j.commatsci.2019.109176.
[56] M.J.D. Powell, A fast Algorithm for Nonlinearly Constrained, (1978).
[57] M. Khan, J. Xu, N. Chen, W. Cao, Asadullah, Z. Usman, D.F. Khan, Effect of Ag doping concentration on the electronic and optical properties of anatase TiO2 a DFT-based theoretical study, Res. Chem. Intermed. 39 (4) (2013) 1633–1644.
[58] A. Angeline Dorothy, N. Ganapathi Subramaniam, P. Panigrahi, Tuning electronic and optical properties of TiO2 with Pt/Ag doping to a prospective photocatalyst a first principles DFT study, Mater. Res. Express 6 (2019), https://doi.org/10.1088/2053-1591/aafc56.
[59] L. Maschio, B. Kirtman, M. Rérat, R. Orlando, R. Dovesi, Ab initio analytical Raman intensities for periodic systems through a coupled perturbed Hartree-Fock/Kohn-Sham method in an atomic orbital basis. I. Theory, J. Chem. Phys. 139 (2013), https://doi.org/10.1063/1.4824442.
[60] D.J. Chadi, Special points for Brillouin-zone integrations, Phys. Rev. B. 16 (1977) 1746–1747, https://doi.org/10.1103/PhysRevB.16.1746.
[61] L. Maschio, B. Kirtman, M. Rérat, R. Orlando, R. Dovesi, Ab initio analytical Raman intensities for periodic systems through a coupled perturbed Hartree-Fock/Kohn-Sham method in an atomic orbital basis. II. validation and comparison with experiments, J. Chem. Phys. 139 (2013), https://doi.org/10.1063/1.4824443.
[62] L. Shi, Z. Zhang, R. Wang, C. Zhou, C. Sun, Synthesis and post-annealing of Ag nanoparticles decorated urchin-like SrTiO3 particles for enhanced electron/hole separation and photocatalytic activity, Ceram. Int. 46 (2020) 19460–19468, https://doi.org/10.1016/j.ceramint.2020.04.294.
[63] V.M. Longo, A.T. de Figueiredo, S. de Lázaro, M.F. Gurgel, M.G.S. Costa, C. O. Paiva-Santos, J.A. Varela, E. Longo, V.R. Mastelaro, F.S. de Vicente, A. C. Hernandes, R.W.A. Franco, Structural conditions that leads to photoluminescence emission in SrTiO3 an experimental and theoretical approach, J. Appl. Phys. 104 (2008), https://doi.org/10.1063/1.2956741.
[64] F.L. Hirshfeld, Bonded-Atom Fragments for Describing Molecular Charge Densities, Theoret. Claim. Acta (Berl.) 44 (2) (1977) 129–138.
[65] D.E.P. Vanpoucke, P. Bultinck, I. van Driessche, Extending Hirshfeld-I to bulk and periodic materials, J. Comput. Chem. 34 (2013) 405–417, https://doi.org/10.1002/jcc.23088.
[66] V.L. Deringer, A.L. Tchougréeff, R. Dronskowski, Crystal orbital Hamilton population (COHP) analysis as projected from plane-wave basis sets, J. Phys. Chem. A 115 (2011) 5461–5466, https://doi.org/10.1021/jp202489s.
[67] L.L. Rusevich, E.A. Kotomin, G. Zvejnieks, A.I. Popov, Ab initio calculations of structural, electronic and vibrational properties of BaTiO3 and SrTiO3 perovskite crystals with oxygen vacancies, Low Temp. Phys. 46 (2020) 1185–1195, https://doi.org/10.1063/10.0002472.